SCIENCE CHINA
Technological Sciences

•Article•

November 2024 Vol.67 No.11: 3499–3512
https://doi.org/10.1007/s11431-024-2710-5

A reduced graphene oxide-coated conductive surgical silk suture targeting microresistance sensing changes for wound healing

DING YuQi[1†], WANG XuChen[1†], LIU JingGe[1], SHEN HongQiang[1], WANG Zhong[1], XIE MaoBin[2], CHEN Ying[3], BARCENAS Adileidys Ruiz[4], ZHAO ZeYu[5*] & LI Gang[1*]

[1]*National Engineering Laboratory for Modern Silk, College of Textile and Clothing Engineering, Soochow University, Suzhou 215123, China;*
[2]*The Sixth Affiliated Hospital of Guangzhou Medical University, Qingyuan People's Hospital; School of Biomedical Engineering, Guangzhou Medical University, Guangzhou 511436, China;*
[3]*Department of Biomedical Engineering, Tufts University, 4 Colby St, Medford MA 02155, USA;*
[4]*National Sericulture Project Research Center in Plant Proteins and Bionatural Products, Havana 11300, Cuba;*
[5]*Department of Applied Physics, The Hong Kong Polytechnic University, Hong Kong 999077, China*

Received March 22, 2024; accepted June 6, 2024; published online October 24, 2024

Conventional sutures used in surgical procedures often lack the capability to effectively monitor physical and chemical activities or the microbial environment of surgical wounds due to their inadequate mechanical properties, insufficient electrical accuracy and unstability. Here, we present a straightforward layer-by-layer coating technique that utilizes 3-glycidoxypropyltrimethoxysilane (CA), graphene oxide (GO), and ascorbic acid (AA) to develop conductive silk-based surgical sutures (CA-rGSFS). The CA-rGSFS feature a continuous reduced graphene oxide (rGO) film on their surface, forming robust hydrogen bonds with silk fibroin. The reduction process of rGO is confirmed through Raman analysis, demonstrating an enhanced D peak to G peak ratio. Notably, the CA-rGSFS exhibit exceptional mechanical properties and efficient electron transmission, with a knot-pull tensile strength of 2089.72 ± 1.20 cN and an electrical conductivity of 130.30 ± 11.34 S/m, respectively, meeting the requirements specified by the United States Pharmacopeia (USP) for 2-0 sutures. These novel CA-rGSFS demonstrate the ability to accurately track resistance changes in various fluid environments with rapid response, including saline, intestinal, and gastric fluids. The suture also retains remarkable stretchablility and stability even after enduring 3000 tensile cycles, highlighting their potential for precise surgical site monitoring during the wound healing process.

layer-by-layer coating, reduced graphene oxide, silk suture, electrical conductivity, microresistance sensing, wound monitoring

Citation: Ding Y Q, Wang X C, Liu J G, et al. A reduced graphene oxide-coated conductive surgical silk suture targeting microresistance sensing changes for wound healing. Sci China Tech Sci, 2024, 67: 3499–3512, https://doi.org/10.1007/s11431-024-2710-5

1 Introduction

Biomedical materials are essential for postoperative wound repair and monitoring to prevent complications like infection, bleeding, dehiscence, and leakage. While various medical solutions, including tapes, clips, screws, glues, adhesives, and wires have been employed in surgical procedures [1], they have limitations such as complex application processes, potential leakage, wound separation upon removal, and substantial development expenses [2–5]. In contrast, sutures remain the cornerstone of surgical management due to their ability to directly close wounds, provide mechanical support, reduce healing time, and minimize inflammation compared to alternative materials [6].

However, conventional sutures lack the capacity to

†Equally contributed to this work.
*Corresponding authors (email: ze-yu.zhao@polyu.edu.hk; tcligang@suda.edu.cn)

perceive physical and chemical activities or monitor the microbial environment of surgical wounds. Recently, researchers have developed sensing sutures integrated with ultrathin electronics, enabling the detection of important parameters related to wound healing or infection, such as temperature, pH, strain, and bacterial counts, for example, Kim et al. [7] designed a smart electronic suture integrated with an ultrathin flexible silicon sensor and a miniature gold heater, allowing accurate temperature measurement for easy monitoring and accelerated wound healing. Lee et al. [8] created a multifunctional electronic suture using a single-fiber core-shell structure with a stretchable conductive fiber core and a drug-containing thermosensitive polymer shell. This suture served as a strain sensor, enabling continuous monitoring of sutured wounds with high sensitivity and mechanical durability. Raza et al. [9] proposed a novel flexible and stretchable wound monitoring sensor based on laser-induced graphene, capable of monitoring various wound parameters such as pH, temperature, and strain.

Despite these advancements, there remain challenges to overcome. The mechanical strength of sutures often decreases significantly due to unfavorable chemical modifications resulting from bioactivity or electronic functionalization [10]. Additionally, there is a lack of effective methods for *in situ* tension measurements of the tissue surrounding the wound after suturing or for assessing the progression of wound healing and mitigating late scarring [11–13]. Although bioelectronic sensors hold promise for providing health monitoring, achieving accurate, stable, continuous, and long-term health monitoring has not yet been fully satisfactory. Therefore, there is an urgent need for innovative functional sutures that can enable timely detection and clinical intervention before complications become severe [14,15].

Silk fibroin (*Bombyx mori*) has extensive utility in biomaterial production for tissue engineering and drug delivery, because of their robust biocompatibility and their good mechanical properties, capacity to avoid causing inflammation or foreign body reactions postimplantation within the human body [16]. Silk has been used in sutures for decades, and through simple weaving and coating methods, tunable mechanical properties and flexible flexibility can be achieved. “Silk has good biocompatibility and is approved by the FDA, which is chosen as suture material [17]”. However, silk sutures lack the functions required to meet the needs of monitoring surgical wounds, such as conductivity and stability. For braided or twisted sutures, coating is a rough surface treatment method for multifilament surgical sutures. Luo et al. [18] demonstrated the feasibility of using reduced graphene oxide (rGO) layers to obtain multifunctional human hair. Coatings can be used to impart antibacterial effects, controlled drug release, or electrical conductivity to suture to compensate for the shortcomings [19].

As a typical two-dimensional (2D) layered material, graphene and its derived materials (including graphene nanosheets, graphene oxide (GO) and rGO) are known for their extraordinary mechanical properties, excellent biocompatibility, cheap synthesis, encompassing fast electron mobility, high current density and large surface area [20–25]. However, due to the poor mechanical properties of single-component GO, which easily leads to electronic failure and severe inflammation, this material cannot meet the complex deformation and biomedical requirements of wound suturing. Although silk fibroin (SF) and rGO materials were combined to develop conductive strategies, Hu et al. [26] used chitosan as a functional finishing agent to perform hydrogen bonding layer-by-layer self-assembly to modify the silk surface. The pure GO coating was easily removed from the silk surface. The particles broke or detached, causing discontinuity in the electrical signal transmission path. Alternatively, silkworms can be fed with mulberry leaves coated with single-walled GO and carbon nanotubes (CNTs) to obtain silk containing single-walled CNTs or GO [27,28]. However, the content of the introduced materials was difficult to control, and it was difficult to reach the threshold for practical application.

According to the Hummers method, potassium permanganate was utilized as an oxidizing agent, along with concentrated sulfuric acid, to synthesize GO from scaled graphite [29], which could be used for large-scale industrial production and the avoidance of toxic gas generation. The graphite oxide flakes display a folded laminated structure, with a significantly higher oxidation degree observed on the surfaces of the flakes. However, GO has poor mechanical properties and is prone to electron failure due to excessive oxygen-containing groups, which cannot meet the needs of conductive sutures. Ascorbic acid (AA) is a water-soluble, green, and environmentally friendly reducing agent [30], which is composed only of carbon, oxygen, and hydrogen atoms that is low risk to introduce heteroatoms and high efficiency to remove oxygen-containing groups, and can be used for green, large-scale, and low-cost production [31]. rGO is produced by the partial reduction of GO with fewer oxygen-containing groups, and rGO achieves high electrical efficiency [32]. rGO has good conductivity and *in vivo* animals experiments reported that there was no deaths of animals, and most existing literatures believed that rGO has blood compatibility [33]. Ma et al. [34] evaluated the impact of exfoliated graphene and polyvinyl alcohol (PVA) nanocomposite fibers and ordinary surgery on wound healing. Through rat trials, it was demonstrated that the healing effect of sutures containing 0.3 wt% is comparable to medical-grade sutures. Tas et al. [35] used a dip-coating method to coat rGO on the surface of polyamide fibers and successfully prepared rGO-coated polyamide monofilament yarns. Their research showed that after seven rounds of dipping in an rGO

solution, the resulting polyamide monofilaments exhibited impressive electrical conductivity. These polyamide monofilaments offered low resistances.

Silk has great potential in the textile industry due to large-scale green production. However, the demand for silk with functional and mechanical properties is also on the rise due to the emergence of other functional textiles. However, at this stage, the large-scale production of silk yarns for conductive functionalization and the application of silk functionalized sutures still remains a great challenge. Chronic wounds are not only difficult to treat and have a long recovery period.

Therefore, it is of great scientific significance and social value to develop and research sutures that can effectively monitor the healing status of wounds. Implanting sensors at the wound site has a high risk of causing inflammation and foreign body reaction, which can worsen the healing process. Therefore, the preparation of silk-based conductive sutures by modifying silk to impart electrical conductivity has great potential in the field of wound monitoring.

In this work, we present electrically conductive functionalized surgical sutures that ensure stable electrical conductivity and improve mechanical strength. The silk sutures were endowed with excellent conductivity and durability by coating them with graphene and modifying them with silane coupling agents. The use of silk fibers for sutures is softer and more firmly knotted than synthetic sutures, and most of the silk sutures have a braided structure, which can greatly improve the mechanical strength of surgical sutures. We tested the electrical conductivity of CA-rGSFS (a straightforward layer-by-layer coating technique that utilizes 3-glycidoxypropyltrimethoxysilane (CA), GO, and AA to develop conductive silk-based surgical sutures) with different additive concentrations of GO, reduction period and impregnation time. The study also analyzed the effect of the coating treatment on the characteristics and properties of surgical sutures such as mass change, thermal behavior, tensile strength and surface morphology. The sutures obtained by this method have stable electrical properties and can be used to detect postoperative complications such as wound infections. CA-rGSFS has great advantages as a functional suture for monitoring the status of wound healing after high-precision surgery.

2 Experimental

2.1 Preparation of GO and rGO solutions

The GO solution was prepared utilizing a modified approach based on the method originally developed by Hummer [29,36,37]. In this procedure, graphite powder (2 g), $NaNO_3$ (2 g), and 98% concentrated H_2SO_4 (50 mL) were mixed in a 1000 mL flask and stirred in an ice bath, maintaining the temperature at 0–5°C. $KMnO_4$ was slowly added in six batches (1 g per batch) to prevent a sudden increase in reaction temperature due to graphite oxidation. The mixture was then transferred to a fume hood and continuously stirred for 2 h using a magnetic stirrer (200 r/min). After removing the mixture from the ice bath, stirring was continued at approximately 25°C for 2 days until the color changed from dark green to a tan paste. The stirred mixture was diluted with deionized water, and 6% H_2O_2 (10 mL) was added to terminate the reaction, resulting in a bright yellow suspension.

For purification, the mixture was repeatedly rinsed with 10% HCl and deionized water. Subsequently, centrifugation was performed at 7500 r/min for 25 min, and the supernatant was discarded. The residue was then washed with deionized water to remove chloride ions until the solution reached neutrality (pH∼7). This process resulted in a well-dispersed GO solution. To prepare rGO materials, AA and GO were mixed in a mass ratio of 10:1.

2.2 Sutures braiding and preparation of CA-rGSFS

The 2-0 suture was created using previously established methods [38]. A 16-spindle automatic braiding machine was utilized, with 16 2×20/22D silk yarns as shell threads and one 2×20/22D and one 2×60/65D (2×20/22D+2×60/65D) as the core wire. The regular braiding structure (2/2 interlacing) was employed, and the braiding speed was set at 60 r/min to ensure consistent tension and avoid breakage during the process (Figure 1(a)). Postprocessing involved ultrasonically cleaning the silk sutures with deionized water at 60°C for 30 min. Subsequently, the treated silk sutures were immersed in a solution of CA in water (silane-to-water volume ratio of 1:15) and soaked at 60°C for 4 h. Afterwards, they were placed in a hot oven and dried at 60°C for 2 h to prepare CA-modified silk sutures (CA-SFS).

A 5 mg/mL aqueous dispersion of GO was prepared and then subjected to ultrasonication for 1 h to ensure thorough dispersion. To ensure full contact between the silk fiber surface and the GO solution, CA-SFS was immersed in the GO solution and left to soak for 2 h. This process was performed prior to the coating process, resulting in the formation of GO-modified CA-SFS (CA-GSFS).

The CA-GSFS was then subjected to an oven at 60°C for a period of 24 h. Additionally, at 80°C, AA was mixed with GO to create an rGO solution. The mass ratio of AA to GO was 10:1. The CA-SFS was placed in a beaker containing the anti-rGO coating and submerged in an 80°C water bath to obtain the rGO-coated silk suture (CA-rGSFS). The silk sutures were subsequently dried at 60°C to complete rGO modification.

To explore the impact of various technological factors on the conductivity of functional medical silk sutures, a three-factor, three-level orthogonal experiment was conducted.

The solution concentration (4, 6 or 8 mg/mL), reduction time (8, 12 or 24 min), and dipping times (4, 6 or 8) were adjusted accordingly (Table 1).

2.3 Surface morphology and structure characterization

The cross-sectional and planar morphologies of the sutures were examined using a benchtop scanning electron microscope (SEM, TM 3030, Hitachi) by observing the secondary electron mode. The samples, with a length of 1 cm, were attached to a conductive adhesive and coated with a layer of gold spray for a duration of 90 s, applying a current of 10 μA and a voltage of 3 kV.

To analyze the secondary structure features of the samples,

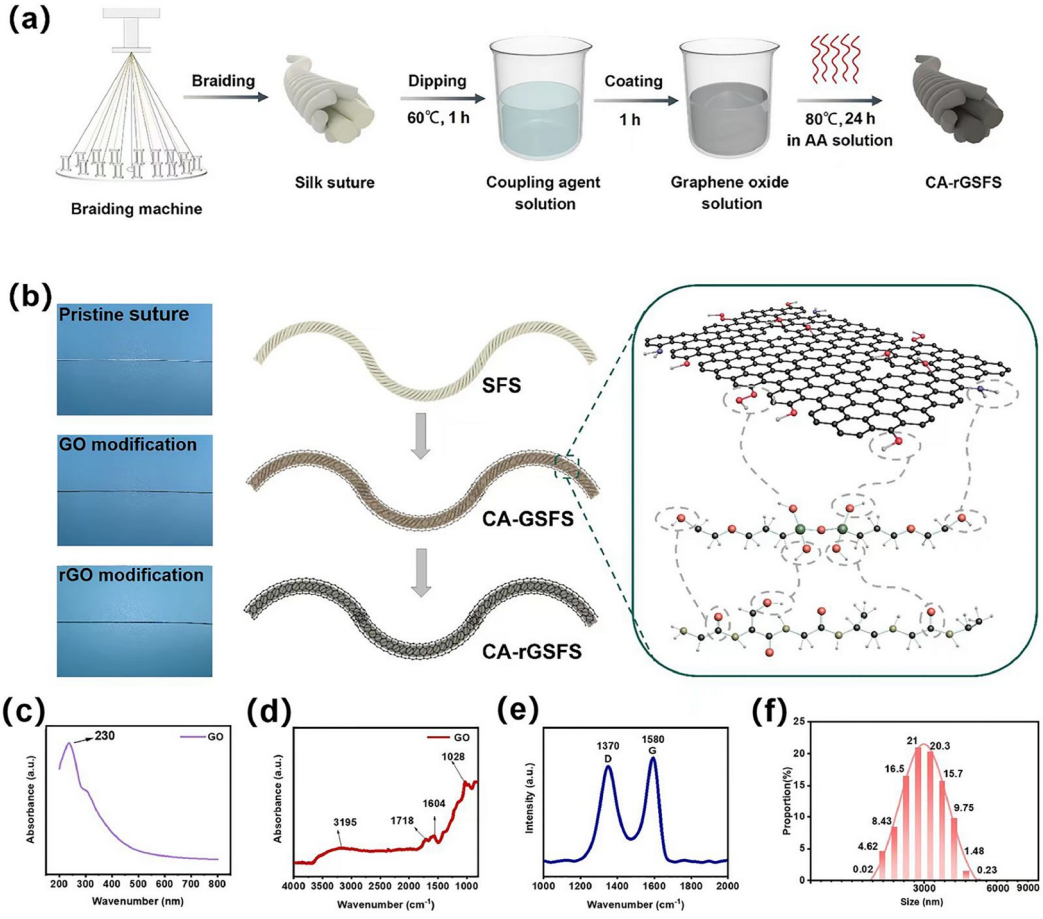

Figure 1 (Color online) Schematic diagram of CA-rGSFS fabrication and characterization of GO solution. (a) Schematic diagram of the CA-rGSFS preparation process; (b) photographs of the SFS, CA-GSFS, and CA-rGSFS, and the schematic diagram of bonding between CA and GO; (c) UV absorption spectra of GO solution; (d) infrared spectra of GO; (e) Raman spectra of GO; (f) particle size of GO solution.

Table 1 Experimental design of the effect of the impregnation treatment process

Sample number	(A) Solution concentration (mg/mL)	(B) Reduction time (min)	(C) Dipping times
1	4	8	4
2	6	24	4
3	8	12	4
4	4	12	6
5	6	8	6
6	8	24	6
7	4	24	8
8	6	12	8
9	8	8	8

a series of scientific techniques were employed. Firstly, the samples were subjected to a cutting and grinding process to obtain a powdered form. Subsequently, a Fourier transform infrared (FTIR) spectrometer (VERTEX 70 + HYPERION 2000, Bruker) was utilized to determine the characteristic absorption peak shifts. The infrared spectra were scanned within the range of 4000–800 cm^{-1}. Additionally, Raman spectroscopy was conducted using a HORIBA XploRA 800 instrument (LabRam) equipped with a 532 nm laser wavelength. A 1200 gr/mm grating was selected, and the filter was adjusted to 25% transmission. The ultraviolet (UV) absorption spectrum of GO solution was measured using a UV-visible spectrophotometer (U-3010, Hitachi) in the range of 200–700 nm at a scan rate of 120 nm/min.

Thermogravimetric analysis (TGA) of the sutures was conducted using a simultaneous DSC-TG Analyzer from TA Instruments. The heating rate was set at 20°C/min, and temperature range was from 30°C to 600°C. The analysis was performed under a nitrogen atmosphere with a flow rate of 10 mL/min.

The particle size distribution of GO was determined using a particle size analyzer (AVANTI J-26S XP, Beckman coulter). The GO solution was diluted to 100 μg/mL and added dropwise to a cuvette until a sufficient amount was achieved. The solution appeared as a light brown-yellow transparent color during observation.

2.4 Evaluation of mechanical and electrical properties of sutures

The mechanical properties of the sutures were evaluated using an Instron-5967 universal material testing machine. The tensile strength of the sutures was measured with a gauge length of 130 mm, utilizing a crosshead speed of 300 mm/min. Additionally, the weight of the sutures was determined using an electronic balance (MP5002, Sunny hengping) with a gauge length of 50 mm. The diameter of the suture was measured at approximately 1/4, 1/2, and 3/4 of the test range section using an electronic thickness gauge adhered to the United States Pharmacopeia (USP) guidelines, providing an accuracy of 0.001 mm. The average value of the measurement was recorded.

The resistance of the suture was measured using a digital multimeter (Keithley DMM7510), and the conductivity was calculated. Silk sutures of 5 cm length were cut, conductive silver paste was used to connect and fix the copper wire and the sample, minimizing the contact resistance between the sample and the electrode (n=5). The conductivity (σ) was calculated according to Eq. (1):

$$\sigma=L/(R\times A), \tag{1}$$

where R represents the resistance of the suture, L represents the length, and A represents the cross-sectional area. A customized tensile module from Kintec Transmission Technology (Suzhou) Co., Ltd. was used to apply a tensile force to the suture. The electrical signals generated by the suture were captured using a Keithley DMM7510 multimeter (Yascon). To facilitate the measurement, copper wires were connected between the suture and the metal probe of the Keithley DMM7510 multimeter. The CA-rGSFS was securely clamped to the linear motor module for testing, which applied a targeted strain to the suture. The resulting electrical signals from the sensor were recorded for further analysis.

To assess the dynamic stability of the CA-rGSFS, strains of 3%, 5% and 7% were applied to the suture using linear motor modules at a frequency of 0.1 Hz and a clamping length of 5 cm. The 3%, 5%, and 7% represent the sutures being stretched to 103%, 105%, and 107% of their original length in each stretch-release cycle, respectively. The frequency of 0.1 Hz represents a stretch-release cycle every 10 s. The changes in the electrical signals were collected during this process. For the static stability test, a strain was applied to the CA-rGSFS, and then the linear motor module operation was immediately stopped once the corresponding strain was reached. The strain was maintained for 80 s at a clamping length of 5 cm, and the changes in the electrical signals were recorded.

To evaluate the durability of the CA-rGSFS, a strain was applied to the suture, and the changes in the electrical signals were recorded after 3000 cycles of stretching. Additionally, the CA-rGSFS was immersed in 50 mL of saline, gastric fluid and small intestinal fluid, respectively, for 5 min. Following immersion, a stretch was applied to the CA-rGSFS, and the changes in the electrical signals were recorded to assess the wet state stability of the suture.

The electromechanical properties of the CA-rGSFS suture were evaluated by investigating its electrical response under cyclic stretching at different strains and frequencies. The rate of change in suture resistance was calculated with the following Eq. (2).

$$(R-R_0)/R_0\times 100\%, \tag{2}$$

where R represents the resistance of the suture in the stretched state, and R_0 represents the resistance of the suture in the unstretched state.

2.5 Statistical analysis

The statistical analysis of the data was performed using the SPSS software. The data are expressed as the mean ± standard deviation (SD). To compare the differences between groups, the one-way analysis of variance (ANOVA) method was applied, and the significance level was determined using the extreme deviation (p) value. If the p-value was greater than 0.05, the difference between the data were considered nonsignificant. If the p-value was less than 0.05, it was considered significant (marked by *), and if p-value was less than 0.01, it was considered highly significant (marked

by **).

The orthogonal test data underwent extreme difference analysis. This analysis was used to determine the influence in each factor on the test results by calculating the *R* value of the extreme difference for each factor. It helped determine the order of the primary and secondary factors and determine the optimal level for each factor by plotting the trend graph of the factor levels.

The initial processing and analysis of the experimental measured data were performed using Microsoft Excel 2019. A table of extreme difference analysis was prepared, and univariate ANOVA was carried out using IBM SPSS 25.0 statistical analysis software. A significance level of $p<0.05$ was considered statistically significant. Graphs were generated using Origin 2018.

3 Results and discussion

3.1 Suture manufacturing and functionalization

Figure 1(a) illustrates the process of functionalizing sutures through coating. Initially, degummed silk was braided using a 16-spindle braiding machine to create SFS, which was then coated with CA to obtain CA-SFS. Subsequently, the sutures were modified with GO solution to obtain CA-GSFS. Finally, CA-GSFS was reduced using a green reducing agent, AA solution, at 80°C to produce CA-rGSFS. Figure 1(b) shows photographs illustrating the physical appearances of the pristine SFS, CA-GSFS, and CA-rGSFS sutures after each respective surface modification process.

In the presence of H_2O, CA undergoes hydrolysis, resulting in the production of hydroxyl groups. The hydroxyl groups form hydrogen bonds with the carbonyl groups of amino acids present in silk fibers [39]. The carbonyl and imide groups on the silk backbone possess dipole moments and serve as active sites for chemical bonding. When the CA-modified SFSs are immersed in the GO solution, the unoccupied hydroxyl groups of CA establish bonds with the carbonyl, carboxyl, epoxide, and hydroxyl groups present on the GO surface. This interaction facilitates the establishment of strong chemical bonds between GO and the substrate. The pristine SFS surface appears fluffier compared to the other surfaces [40]. In contrast, the functionalized SFS undergoes volume shrinkage, facilitating the formation of a dense of GO structure on the fiber surface. This results in the creation of an efficient electron transport pathway, leading to high electrical conductivity [41].

The spectrum of the GO solution exhibits a characteristic UV peak near 230 nm (Figure 1(c)), which corresponds to the π-π transition absorption of C=C on the aromatic ring within the GO molecule [42]. This peak confirms the successful preparation of the GO solution using the Hummers method. Figure 1(d) displays significant characteristic peaks of GO near 3195, 1718, 1604, and 1028 cm^{-1}. The strong peak at 3195 cm^{-1} is attributed to the oscillation of the O–H bond, indicating the presence of a large number of hydroxyl groups in GO. The peak near 1718 cm^{-1} represents the C=O stretching vibration, while the peak at 1604 cm^{-1} arises from the combined effects of water vibration between GO layers and the backbone vibration in unoxidized GO. The peak near 1028 cm^{-1} corresponds to the absorption frequency of C–O bonds [43]. These characteristic peaks confirm the successful preparation of GO by the Hummers method.

Figure 1(e) shows significant characteristic peaks of GO near 1370 and 1580 cm^{-1}. The D peak at 1370 cm^{-1} is primarily attributed to structural defects and atomic doping in GO, while the G peak at 1580 cm^{-1} arises from the in-plane vibration of the sp^2 carbon atoms [44]. These peaks further validate the successful use of the Hummers method in preparing GO. In Figure 1(f), the flake size distribution of GO ranges mainly between 3 and 6 μm. This indicates that the GO flakes in the prepared GO solution possess uniform sizes, facilitating the uniform coverage of the silk suture surface when impregnated with the GO solution, The uniform coating enables the formation of more electron transport paths, thereby improving the electrical conductivity of the sutures.

3.2 Characterizations of the CA-rGSFS

FTIR spectroscopy was utilized to investigate the interfacial interactions between the coated rGO layer and CA-SFS (Figure 2(a)). The most noticeable difference was observed at 1060 cm^{-1}, corresponding to the stretching vibrations of Si–O–Si [45]. Upon treatment with AA, the FTIR spectrum of CA-rGSFS exhibited significant changes, including weaker peaks at 3285, 2925, 1625, and 1510 cm^{-1}, indicating successful reduction of GO to rGO on the suture surface [46]. The peak at 3285 cm^{-1} represented O–H and N–H stretching vibrations, and its intensity was lower in the rGO coating compared to GO, suggesting a reduction in GO content [47]. Figure 2(b) demonstrates the conductivity test results of the CA-rGSFS prepared using an orthogonal test protocol. Among them, samples 1, 4, and 7 were impregnated with GO at a concentration of 4 mg/mL, samples 2, 5, and 8 were impregnated with GO at a concentration of 6 mg/mL, and samples 3, 6, and 9 were impregnated with GO at a concentration of 8 mg/mL. As shown in the figure, the highest conductivity of the sutures is achieved when the number of coatings is 8 and the concentration of GO is 8 mg/mL, whereas with the decrease of the concentration of GO impregnation, the conductivity decreases from 130.30 ± 11.34 to 55.77 ± 7.18 S/m at a GO impregnation concentration of 4 mg/mL. At the same concentration, the reduction time exhibits significant increase at 24 min, while there is no significant difference between 8 and 12 min. Additionally, a

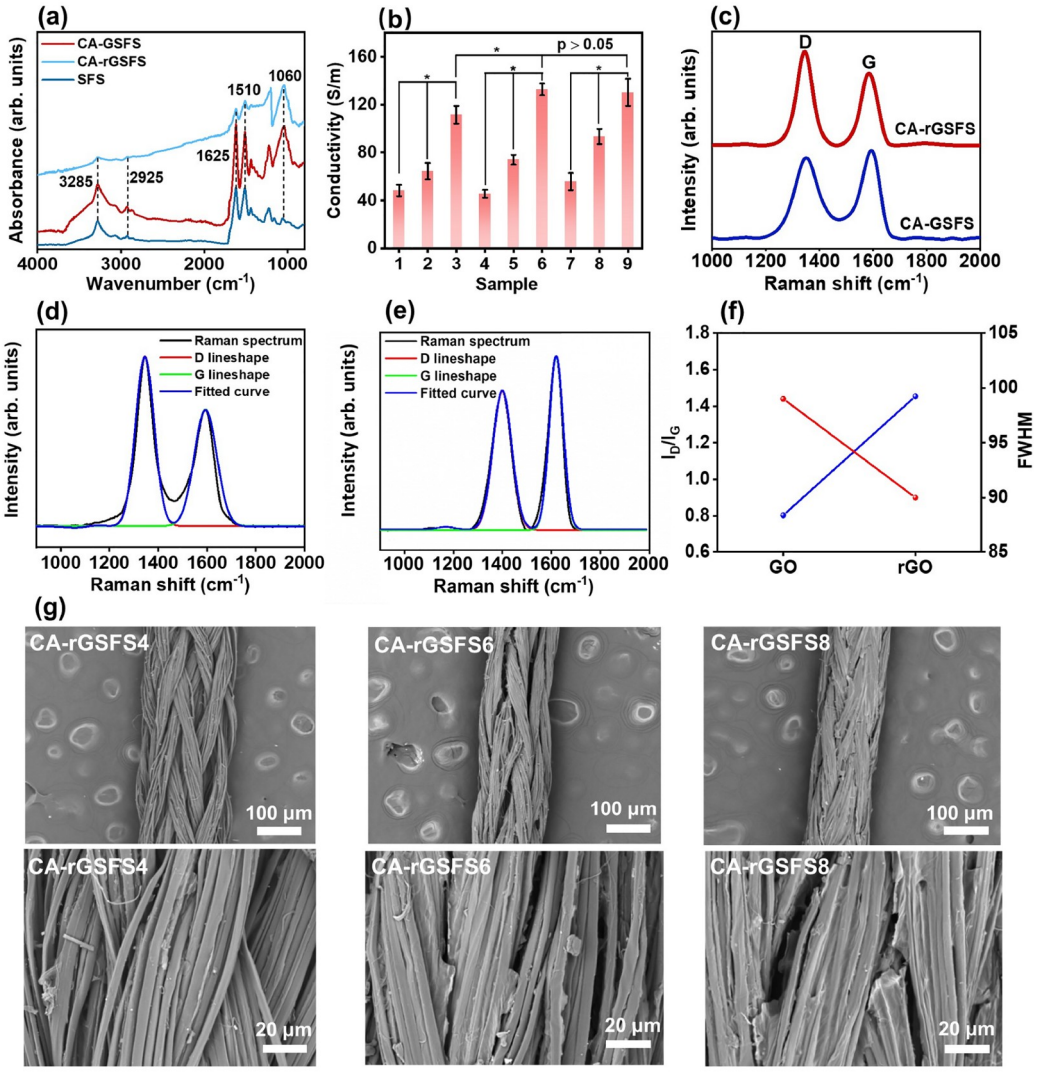

Figure 2 Characterization of the SFS, CA-GSFS and CA-rGSFS. (a) FTIR spectra of the SFS, CA-GSFS, and CA-rGSFS; (b) conductivity of the CA-rGSFSs; (c) Raman spectra of the CA-GSFS and CA-rGSFS; (d) fitting peak of the CA-GSFS Raman spectra; (e) fitting peak of the CA-rGSFS Raman spectra; (f) ratio of the D and G peaks and FWHM of CA-GSFS and CA-rGSFS; (g) SEM images of the different coating times of CA-rGSFSs (100 and 20 μm).

significant difference is observed between 4 and 6 immersion times, but there is no significant difference for 8 times. On the other hand, when the GO impregnation concentration was 8 mg/mL, the conductivity of the suture increases from 111.51 ± 6.79 to 130.30 ± 11.34 S/m as the number of coatings increased. It is evident that the CA-rGSFS obtained superior electrical conductivity with more rGO coverage and bonding because of the strong π-π interactions formed between neighboring rGO, creating interconnected electron transport paths [48]. In order to explore the correlation between sample resistance and the number of functional coating times, we conducted experiments using 4, 6, and 8 coating cycles on the sutures, which were labeled as CA-rGSFS4, CA-rGSFS6, and CA-rGSFS8. With the increasing number of the dipping times, the conductivity dramatically increased. Additionally, the conductivity of rGSFS is lower than that of CA-rGSFS, indicating that the presence of the CA coating led to an enhancement in electrical conductivity [49]. After the rGO functionalized, the electrical conductivity is increased (CA-rGSFS4, CA-rGSFS6 and CA-rGSFS8, 111.51 ± 7.39, 132.83 ± 5.01 and 130.30 ± 11.34 S/m, respectively), making it possible to be used in wound monitoring. The enhanced electrical conductivity could be attributed to the transformation of σ bonds in GO to π bonds in rGO. In other words, more free electrons are released through the suture as some of the oxygen groups are removed during the reduction process.

The Raman spectra of CA-GSFS and CA-rGSFS are shown in Figure 2(c), which verified the reduction of rGO on the suture surface. The Raman peaks observed at 1370 cm^{-1} (attributed to defects or heteroatom-doping) and 1580 cm^{-1} (related to the sp^2-bonded crystalline carbon's vibrations),

corresponding to the disorder-induced D-band and tangential G-band [50]. The intensity ratio of the D-band to the G-band increases from 0.8 to 1.4 (Figure 2(d) and (e)), while the half-width-to-height ratio (FWHM) decreases from 99 to 90 (Figure 2(f)). The enhanced D peak indicated the formation of small-sized sp^2 bonds in GO during the reduction process, while the reduced FWHM indicates an increase in the ordered structure of rGO [51]. This reduction process leads to a decrease in the size of the sp^2 structural domains and a transition from the sp^2 to sp^3 domains, resulting in structural defects [52]. The decrease in the I_D/I_G value of GO is attributed to the partial removal of the oxygenated functional groups. This removal enables a strong binding interaction between CA and GO through substitution between the remaining oxygenated functional groups on GO and the hydroxyl group of hydrolyzed CA [46].

SEM images from the top view (80×) and magnification (500×) of in Figure 2(g) reveal the surface characteristics of the sutures with different coating times. Sutures with fewer coating times exhibit a rough, loose surface with numerous tiny pores, while those with more coating period display a smoother surface with fewer pores and closer inter fiber contact, indicating an increase amount of rGO on the silk suture with higher coating times [40].

To quantitatively assess the conformational changes arising from the interactions between CA and silk fibroin during surface modification, FTIR spectroscopy was employed to deconvolve the spectra within 1700–1600 cm^{-1} (amide I zone) for both SFS and CA-SFS (Figure 3(a) and (b)) [53]. The analysis reveals a significant enhancement in the β-sheet structure, suggesting that CA likely plays a pivotal role in promoting the generation of β-sheet structures within silk fibroin through hydrogen bonding with silk, as illustrated in Figure 3(c) [54].

The thermal stability of the samples was investigated in order to test the effect of the number of impregnations on the

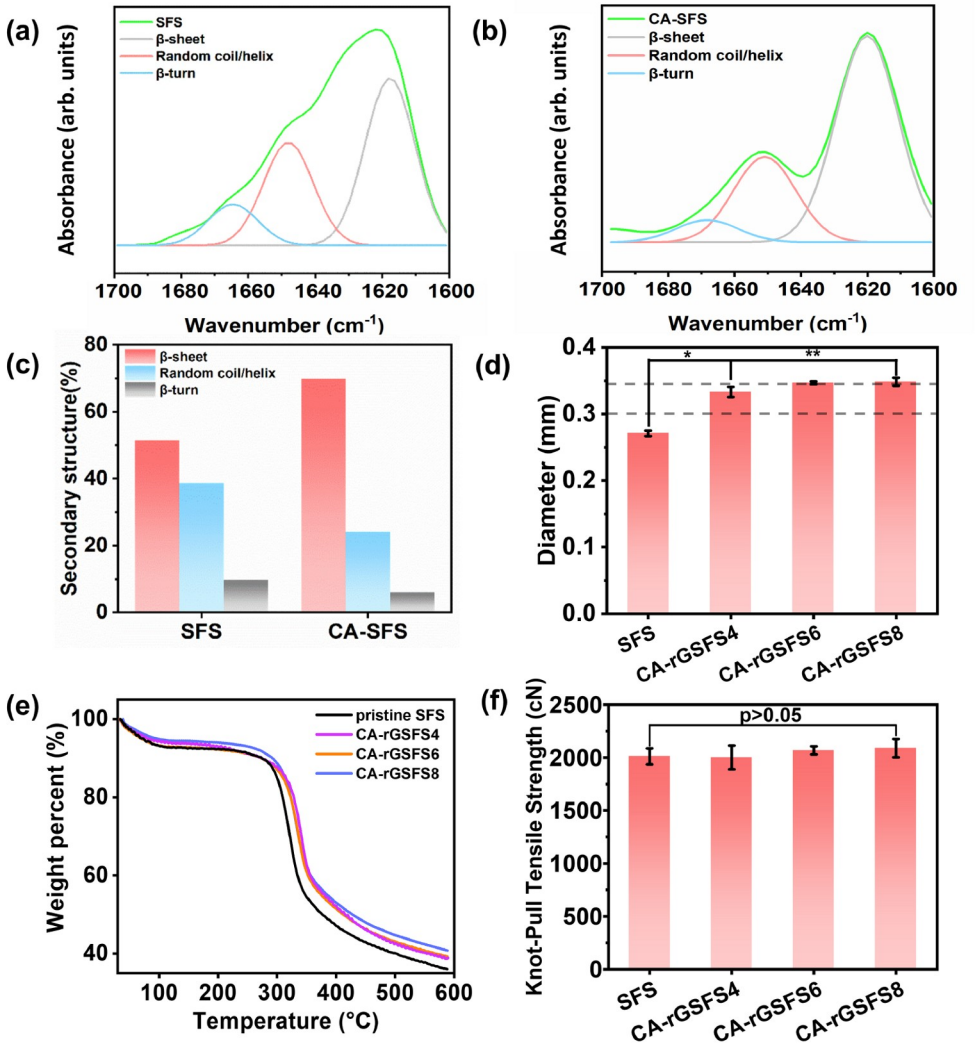

Figure 3 Characterization of structure and physical changes of SFS, CA-SFS and CA-rGSFS. Deconvolved FTIR spectra of the SFS (a) and (b) CA-SFS; (c) conformational changes of the SFS and CA-SFS; (d) diameters of the SFS, CA-rGSFS4, 6 and 8; (e) TG curves of the SFS, CA-rGSFS4, 6 and 8; (f) knot-pull tensile strengths of the SFS, CA-rGSFS4, 6 and 8.

conductivity of the sutures, as shown in Figure 3(e), with an increase in temperature from 30°C to 600°C, the samples experienced a weight loss of approximately 60%. However, the samples coated with rGO modification shows slightly less weight deterioration upon heating [48]. At 100°C, the CA-rGSFS displays a small mass loss primarily due to evaporative loss of water inside the sutures. As the temperature approached approximately 300°C, the mass loss of SFS became more pronounced [55], mainly due to thermally induced damage in the silk fibroin. Conversely, the CA-rGSFS, after undergoing impregnation treatment, exhibits a uniform coating of rGO on the suture surface, which provided thermal protection. Consequently, the weight loss of CA-rGSFS8 is smaller than that of CA-rGSFS4 and CA-rGSFS6, owing to the higher rGO content in CA-rGSFS8, resulting in improved thermal stability. Moreover, an increase in the number of impregnation times led to subsequent increases in the rGO content on the surface of the silk suture, thereby enhancing the electrical conductivity [56].

The physical and mechanical properties were evaluated to comply with the USP standard. As shown in Figure 3(d), the diameters of the samples are in line with the 2-0 suture range of 0.300–0.349 mm. Even though the individual values show an increasing trend as dipping times increase (SFS, CA-rGSFS4, CA-rGSFS6 and CA-rGSFS8 are 0.271 ± 0.004, 0.348 ± 0.007, 0.347 ± 0.002 and 0.343 ± 0.006 mm respectively), all the coated sutures are between the value ranges specified by the standard [57]. The mechanical properties of the sutures are shown in Figure 3(f). The knot-pull tensile strength of the pristine suture increases (SFS, 2012.42 ± 0.56 cN) as number of coating times increases (CA-rGSFS4, CA-rGSFS6 and CA-rGSFS8, 2001.64 ± 1.13, 2069.16 ± 0.38, 2089.72 ± 1.20 cN), and all the sutures exceed the standard requirement (2-0 suture, ≥1020 cN). It shows that the rGO modification effectively improves the mechanical properties of SFS, which may also confirm the "hydrogen bond" strengthening network. In the coated rGO interface layer, CA provides a number of hydroxyl and amino groups, which could form a hydrogen bond between the rGO and silk [58] and plays an interfacial reinforced role in the structure.

3.3 Electrical performance

The electrical properties of fiber materials are crucial for their functional applications [59]. Silk fiber offers several advantages, such as affordability, environmental friendliness, biocompatibility, and scalability [60,61]. However, the silk industry has faced challenges regarding future applications, making it difficult to meet the demand for functional textiles, especially those with electrical functionality, in emerging markets [62]. To address this, a functionalized layer of rGO was incorporated onto silk fiber, resulting in a significant increase in electrical conductivity to 130.30 ± 11.34 S/m. This enhancement makes silk fiber suitable for applications in smart textiles and wearable electronics. By coating silk fiber with a thin layer of GO, known as CA-rGSFS fiber, they become an intriguing material for the electronics industry because of their desirable material properties. The enhanced electrical conductivity of reduced sutures could be attributed to the transformation of σ bonds in GO to π bonds in rGO, which leads to the release of more free electrons as certain oxygen groups are removed during the reduction process.

Figure 4(a) illustrates the dynamic strain stability of CA-rGSFS by subjecting it to periodic stretching–releasing cycles at a frequency of 0.1 Hz, specifically at strain levels of 3%, 5%, and 7%. The consistent electrical outputs observed at each strain level validate the sutures' dynamic stability [63]. When the stretched strain exceeds 7%, the suture fails to recover its initial length promptly after the cycle's end, resulting in slight relaxation [64]. Consequently, the electronic response of the suture fluctuates from relaxation to elongation at the beginning of the next cycle. However, when the sensor experiences tensile strains of 3%, 5%, and 7%, the electrical signal quickly stabilizes with slight overshooting (Figure 4(c)), illustrating the outstanding static stability of the CA-rGSFS [65]. The effects of wet environments are also investigated on the sutures. As shown in Figure 4(b), the influence of the moist conditions on the sensitivity of the suture is relatively minimal, suggesting that the sutures remain functional even in real-world usage scenarios. The stability of properties relies heavily on efficient interfacial interactions.

GS fibers, which are silk fibers coated with GO, exhibit notable deformation when incorporated into textiles and subjected to daily usage [66]. Therefore, it is essential to assess the stability and durability of GS fibers under realistic circumstances to evaluate their practical usability as functional sutures. To achieve this, a 3% cyclic strain was applied at 0.1 Hz for 3000 cycles. The electronic signals exhibit stability throughout the entire cycle, with minor fluctuations, as shown in Figure 4(d)–(f). This indicates that the conductivity of CA-rGSFS is well-maintained even after undergoing repeated deformation, and both are stretched; the conductivity of CA-rGSFS sutures remains at 95% after 3000 cycles, demonstrating the reliability of these sutures for practical applications [67]. Furthermore, the electrical conductivity is consistently maintained, indicating strong adhesion between the rGO functional layer and SFS during the deformation process. An intriguing finding is that the conductive CA-rGSFS could detect deformation, which could be advantageous for developing stimuli-responsive textiles. As depicted in Figure 4(d)–(f), stretching the CA-rGSFS caused the separation of rGO in the functionalizing layer, resulting in increased resistance. Conversely, when the CA-rGSFSs

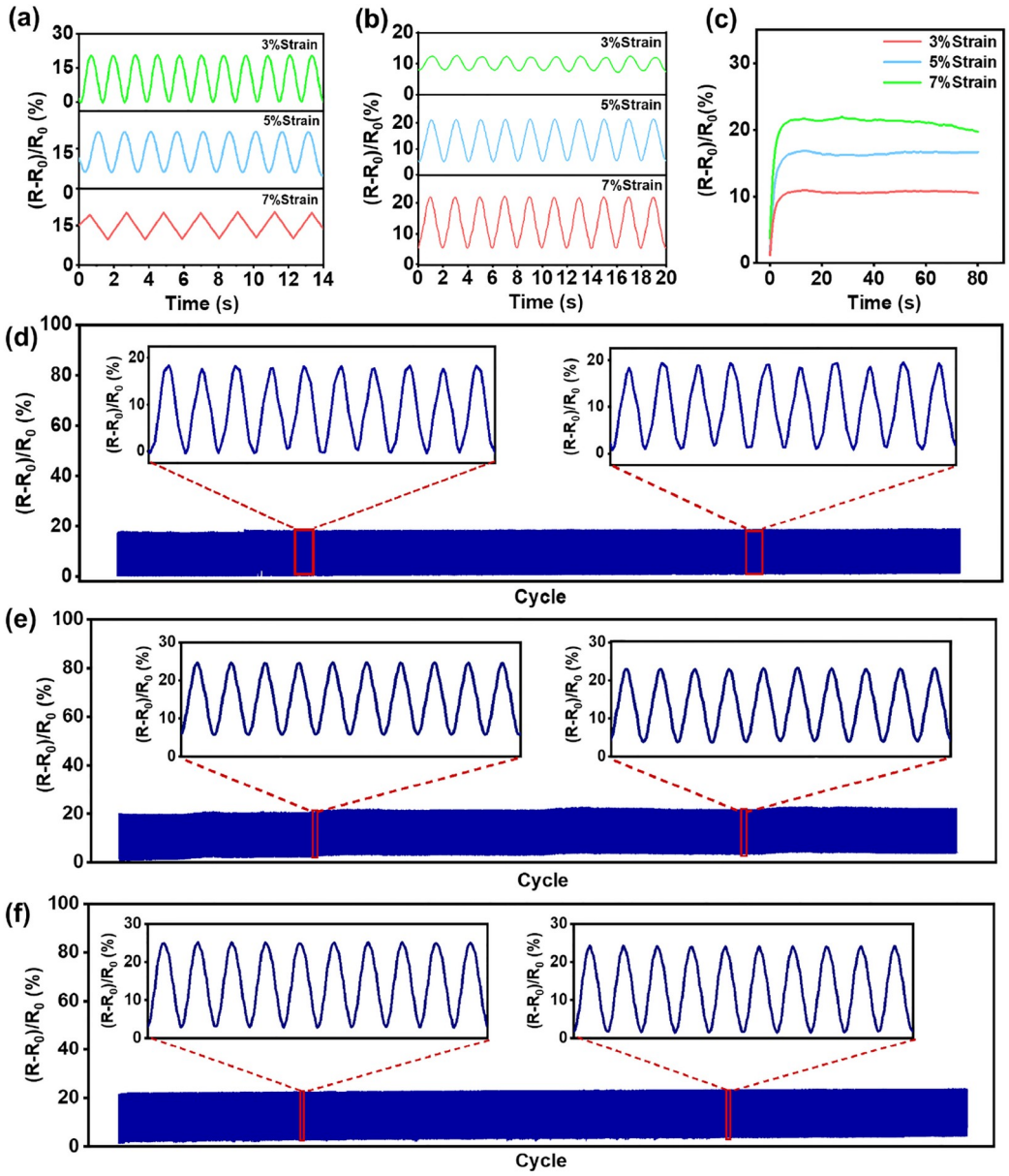

Figure 4 Electromechanical performance of the CA-rGSFS suture. Dynamic stability of the suture at strain levels of 3%, 5%, and 7% and a frequency of 0.1 Hz, in (a) dry and (b) humid environments; (c) static stability of the suture at strain levels of 3%, 5%, and 7%. Electrical responses of (d) the CA-rGSFS4, (e) the CA-rGSFS6, and (f) the CA-rGSFS8 with 3% cyclic strain applied, 0.1 Hz frequency, and 3000 cycles.

return to its original state, both the functionalizing layer and the resistance return to their initial states. Importantly, these changes exhibit excellent repeatability during 3% strain cycles, highlighting the promising application of the CA-rGSFS as a wound monitor.

After the GO in CA-rGSFS was reduced to rGO by AA, the σ bond was converted to the π bond in rGO, resulting in the reduction or removal of hydrophilic oxygen-containing groups including hydroxyl and carboxyl groups [54,68]. Therefore, CA-rGSFSs were less affected by liquids and electrical signals could be stably output. Moreover, a hopping transmission of carriers occurs within the GO and rGO structures [69]. The reduction of oxygen-containing groups led to a sharp decrease in the amount of hopping charge transmission, promoting a lower density of activated deep trap states and short-range variable hopping of carriers between adjacent layers of rGO [70,71]. Although the presence of a liquid environment could promote the generation of charge carriers, the number of hopping charge transmissions decreased [72,73]. Consequently, in a liquid environment, there is an increased transmission and release of free electrons, resulting in enhanced conductivity and maintenance of a highly stable and repeatable electrical response and signal pattern, which remains unaffected by changes in the liquid

environment. These findings indicate that the functional sutures can serve not only as conventional wound sutures but also as novel tools for continuous health monitoring without impeding daily activities. In the field of biomedical applications, they can effectively track variations in wound temperature or deformation, thereby facilitating postoperative care and managing chronic disease. Furthermore, the CA-rGSFS exhibited remarkable reliability and accuracy in wound motion analysis and rehabilitation monitoring functions, further enhancing their utility [74].

3.4 Applications

Figure 5(a) and (b) illustrate the effect of various tensile strains (3%, 5%, and 7%) on suture resistance in the intestinal and gastric fluid environments. The CA-rGSFS shows the ability to respond appropriately under these dynamic conditions, producing stable signals. The rate of change of resistance of the CA-rGSFS in the intestinal fluid environment (pH~1) is slightly greater than that in the gastric fluid environment (pH~8). These findings suggest that sutures have potential for *in vivo* applications and human wound monitoring [75].

Figure 5(c) and (d) illustrate the process of suture testing on the custom tensile module and data transfer to the computer. Figure 5(e) demonstrates the proof-of-concept for advanced wound management, showing how suture sensing networks can enable data acquisition, transfer, visualization, anomalous event detection, and early warning. The wireless and battery-free CA-rGSFS technology enables continuous sensing without compromising the mechanical properties of the sutures. Extensive mechanical and electromagnetic

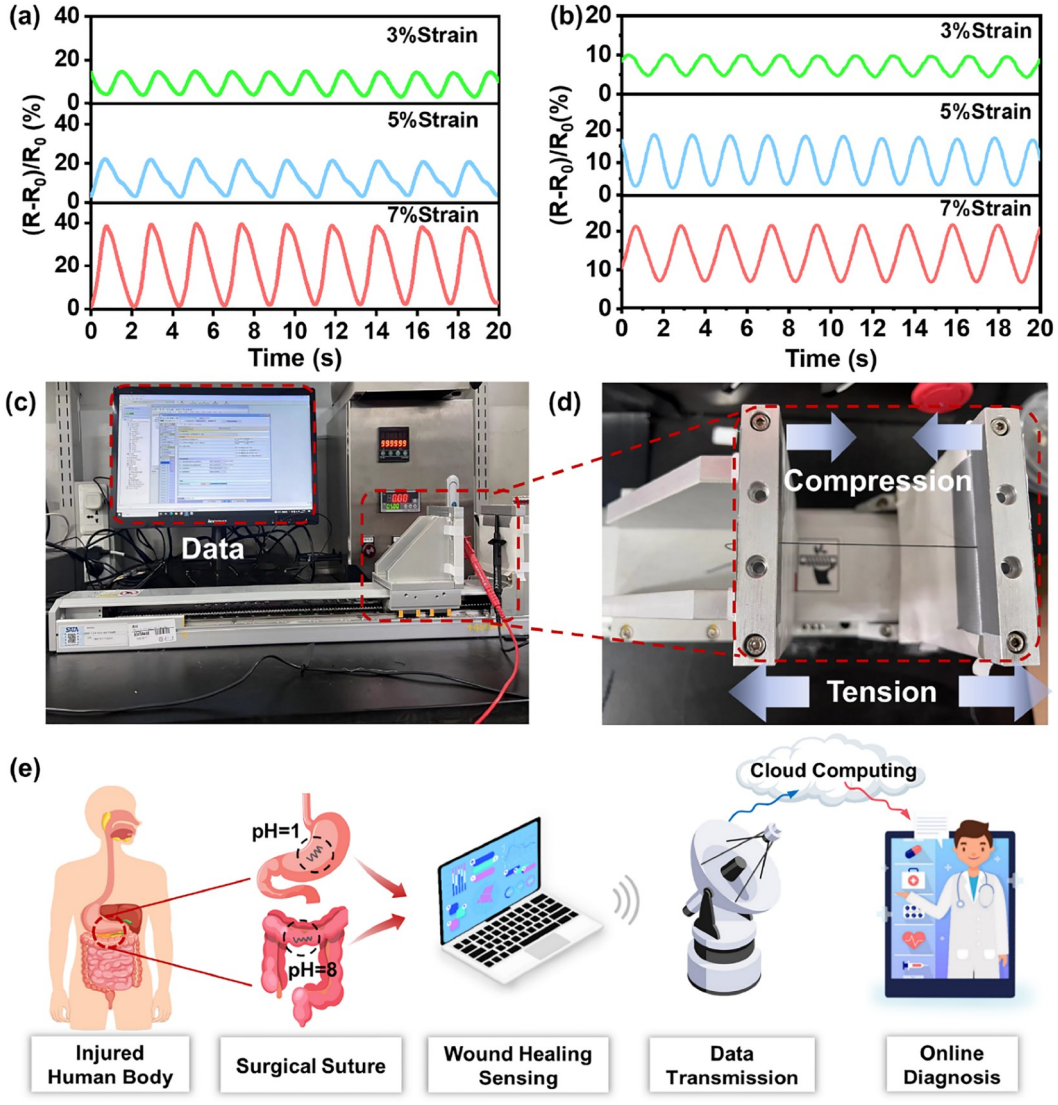

Figure 5 (Color online) Applications of the CA-rGSFS in wound healing sensing networks. Changes in the resistance of CA-rGSFS at different strains from 3%, 5%, and 7% in (a) intestinal and (b) gastric environment; (c) photo of customized tensile module and data transferred to the computer; (d) photographs of CA-rGSFS tested on customized tensile module; (e) demonstration of a proof-of-concept for a remote point-of-care sensing system that utilizes sutures and a big data diagnostic system for advanced wound management.

investigations have established the operational characteristics of wireless sensing systems, making them suitable for various suture types, surgical sutures, and anatomical regions. By offering continuous monitoring of deep surgical sites, these wireless sutures could potentially complement or replace existing nonabsorbable sutures, clips, and staples. Removal of the sutures can be performed through subsequent surgical or endoscopic procedures once the risk of complications has subsided or if the sutures are intended to remain in the body indefinitely. However, further validation of the sutures' long-term wireless functionality, particularly in postoperative monitoring, as well as their long-term biocompatibility, is necessary to establish their suitability for medical-grade suture performance.

To enable large-scale production, the improved Hummers method is utilized to synthesize GO, effectively avoiding the generation of toxic gases [31]. The reduction of GO is achieved through the use of a green agent, resulting in improved production efficiency and cost reduction [24]. The sutures are braided using an improved technology to achieve a core shell structure to improve mechanical properties [57], and through standardized process large-scale production can be achieved. The conductive functional sutures are prepared through a layer-by-layer coating process, which is simple, convenient, operable, and suitable for industrial production and provides support for the transformation and upgrading of the textile industry.

The negative durability, response, and sensing reliability (temperature, humidity) of various sensor systems are summarized and compared (Table 2). It can be found that many previous foam and hydrogel sensor systems (such as GO, MXene) have enhanced mechanical strength and conductivity, can withstand high temperatures [76] or freezing [77], and have cyclically repeated stability at different temperatures. After freezing, the hydrogel would inevitably deform during repeated mechanical processes, the sensor signal will drift slightly, and it is sensitive to humidity changes [76–78]. In the yarn of fiber-based electronic (MWCNT) sensing devices, the strain sensing network is unclear about the change in humidity, has high reliability in humidity, but still changes in liquid environments, and the addition of water will affect the sensing performance [49,79]. Notably, knitted cotton and polyester fabric sensor systems (rGO) show a negative response under humidity, with almost no frequency dependence [50,80]. Our results show that CA-rGSFS has improved cyclic stability under liquid and has a good negative response, which is better than previous materials. The significance of these results consists in the fact that the layer-by-layer coating of CA-rGSFS is an ideal choice for stable monitoring under wet state.

4 Conclusions

In summary, we developed a conductive silk suture functionalized with rGO, exhibiting high sensing stability and resilience to humidity changes. The GO solution was uniformly prepared using the Hummers method, and the rGO was obtained through an environmentally friendly AA reducing process. The combination of silk sutures and rGO was achieved using CA, which not only facilitated excellent hydrogen bonding but also ensured thermal stability while meeting the diameter and mechanical property requirements outlined by USP for 2-0 sutures. The most significant achievement of this research lies in the suture's exceptional conductivity, reliability, and accuracy. It demonstrates rapid response and cycle repetition stability, maintaining uniform resistance changes even under varying mechanical forces and wet conditions. Additionally, the suture exhibits stability in simulated gastric and intestinal body fluids. This novel CA-rGSFS holds great potential for stable and continuous sensing of wound deformation, thereby benefiting postoperative diagnosis, rehabilitation exercises, and monitoring applications. Ultimately, it has the potential to reduce postoperative hospitalization interventions and minimize interference with daily life activities.

Table 2 Comparison of durability, negative response and sensing reliability of sensor systems[a)]

Sensing systems	Coefficient of determination (R^2) (%)	Durability	Negative response	Sensing reliability in temperature	Sensing reliability in humidity	Refs
Cellulose/MXene/PDMS foam	–	10 cycles under the strain of 50%	×	√	–	[76]
AM/CS/GO hydrogel	99.6	200 cycles under the strain of 200%	×	√	–	[77]
AM/CS/MXene hydrogel	–	50 cycles under the strain of 200%	×	√	–	[78]
AM/cellulose/MXene hydrogel	–	100 cycles under the strain of 60%	×	–	√	[79]
MWCNT/Ecoflex yarn	98.92	2000 cycles under the strain of 6%	×	√	√	[49]
rGO/wool fabric	–	500 cycles under a frequency of 0.5 Hz	×	√	√	[50]
rGO/polyester fabric	–	500 cycles under the strain of 7.5%	√	–	–	[80]
rGO/silk suture	–	3000 cycles under the strain of 7%	√	–	√	This work

a): MXene: 2D transition metal carbide, nitride, or carbonitride; PDMS: polydimethylsiloxane; MWCNT: multi-walled CNT; AM: acrylamide; CS: chitosan; GO: graphene oxide; rGO: reduced graphene oxide.

This work was supported by the National Natural Science Foundation of China (Grant No. 82374295). We are also thankful for the support of the National Key R&D Program of China (Grant No. 2021YFE0111100), the Science and Technology Partnership Program by the Ministry of Science and Technology of China (Grant No. KY202201002), Jiangsu Provincial Department of Science and Technology (Grant No. BZ2022017), and China National Textile and Apparel Council (Grant No. J202002).

Funding note Open access funding provided by Hong Kong Polytechnic University.

1 Scognamiglio F, Travan A, Rustighi I, et al. Adhesive and sealant interfaces for general surgery applications. J Biomed Mater Res, 2016, 104: 626–639
2 Jain R, Wairkar S. Recent developments and clinical applications of surgical glues: An overview. Int J Biol Macromolecules, 2019, 137: 95–106
3 Gallo A L, Paladini F, Romano A, et al. Efficacy of silver coated surgical sutures on bacterial contamination, cellular response and wound healing. Mater Sci Eng-C, 2016, 69: 884–893
4 Baygar T, Sarac N, Ugur A, et al. Antimicrobial characteristics and biocompatibility of the surgical sutures coated with biosynthesized silver nanoparticles. Bioorg Chem, 2019, 86: 254–258
5 Joseph B, George A, Gopi S, et al. Polymer sutures for simultaneous wound healing and drug delivery—A review. Int J Pharm, 2017, 524: 454–466
6 Iqbal N, Khan A S, Asif A, et al. Recent concepts in biodegradable polymers for tissue engineering paradigms: A critical review. Int Mater Rev, 2019, 64: 91–126
7 Kim D H, Wang S, Keum H, et al. Thin, flexible sensors and actuators as 'instrumented' surgical sutures for targeted wound monitoring and therapy. Small, 2012, 8: 3263–3268
8 Lee Y, Kim H, Kim Y, et al. A multifunctional electronic suture for continuous strain monitoring and on-demand drug release. Nanoscale, 2021, 13: 18112–18124
9 Raza T, Tufail M K, Ali A, et al. Wearable and flexible multifunctional sensor based on laser-induced graphene for the sports monitoring system. ACS Appl Mater Interfaces, 2022, 14: 54170–54181
10 Xu L, Liu Y, Zhou W, et al. Electrospun medical sutures for wound healing: A review. Polymers, 2022, 14: 1637
11 Mir M, Ahmed N, Permana A D, et al. Enhancement in site-specific delivery of carvacrol against methicillin resistant staphylococcus aureus induced skin infections using enzyme responsive nanoparticles: A proof of concept study. Pharmaceutics, 2019, 11: 606
12 Liu M, Zhang Y, Liu K, et al. Biomedical devices: Biomimicking antibacterial opto-electro sensing sutures made of regenerated silk proteins. Adv Mater, 2021, 33: 2170002
13 Rippa A L, Kalabusheva E P, Vorotelyak E A. Regeneration of dermis: Scarring and cells involved. Cells, 2019, 8: 607
14 Aarabi S, Bhatt K A, Shi Y, et al. Mechanical load initiates hypertrophic scar formation through decreased cellular apoptosis. FASEB J, 2021, 21: 3250–3261
15 Ogawa R. Mechanobiology of scarring. Wound Repair Regeneration, 2011, 19: s2
16 Liu J, Huang R, Li G, et al. Generation of nano-pores in silk fibroin films using silk nanoparticles for full-thickness wound healing. Biomacromolecules, 2021, 22: 546–556
17 Ghalei S, Handa H. A review on antibacterial silk fibroin-based biomaterials: Current state and prospects. Mater Today Chem, 2022, 23: 100673
18 Luo C, Zhou L, Chiou K, et al. Multifunctional graphene hair dye. Chem, 2018, 4: 784–794
19 Debbabi F, Gargoubi S, Hadj Ayed M A, et al. Development and characterization of antibacterial braided polyamide suture coated with chitosan-citric acid biopolymer. J BioMater Appl, 2017, 32: 384–398
20 Du X, Skachko I, Barker A, et al. Approaching ballistic transport in suspended graphene. Nat Nanotech, 2008, 3: 491–495
21 Nair R R, Blake P, Grigorenko A N, et al. Fine structure constant defines visual transparency of graphene. Science, 2008, 320: 1308
22 Balandin A A, Ghosh S, Bao W, et al. Superior thermal conductivity of single-layer graphene. Nano Lett, 2008, 8: 902–907
23 Lee C, Wei X, Kysar J W, et al. Measurement of the elastic properties and intrinsic strength of monolayer graphene. Science, 2008, 321: 385–388
24 Zhu Y, Murali S, Cai W, et al. Graphene and graphene oxide: Synthesis, properties, and applications. Adv Mater, 2010, 22: 3906–3924
25 Suzuki S, Yoshimura M. Chemical stability of graphene coated silver substrates for surface-enhanced raman scattering. Sci Rep, 2017, 7: 14851
26 Hu X, Ren N, Chao Y, et al. Highly aligned graphene oxide/poly(vinyl alcohol) nanocomposite fibers with high-strength, antiultraviolet and antibacterial properties. Compos Part A-Appl Sci Manufacturing, 2017, 102: 297–304
27 Wang Q, Wang C, Zhang M, et al. Feeding single-walled carbon nanotubes or graphene to silkworms for reinforced silk fibers. Nano Lett, 2016, 16: 6695–6700
28 Qu J, Dai M, Ye W, et al. Study on the effect of graphene oxide (GO) feeding on silk properties based on segmented precise measurement. J Mech Behav BioMed Mater, 2021, 113: 104147
29 Yoo M J, Park H B. Effect of hydrogen peroxide on properties of graphene oxide in Hummers method. Carbon, 2019, 141: 515–522
30 Palomba M, Carotenuto G, Longo A. A brief review: The use of *L*-ascorbic acid as a green reducing agent of graphene oxide. Materials, 2022, 15: 6456
31 De Silva K K H, Huang H H, Joshi R K, et al. Chemical reduction of graphene oxide using green reductants. Carbon, 2017, 119: 190–199
32 Mahmood H, Tripathi M, Pugno N, et al. Enhancement of interfacial adhesion in glass fiber/epoxy composites by electrophoretic deposition of graphene oxide on glass fibers. Compos Sci Tech, 2016, 126: 149–157
33 Pinto A M, Gonçalves I C, Magalhães F D. Graphene-based materials biocompatibility: A review. Colloids Surfs B-Biointerfaces, 2013, 111: 188–202
34 Ma Y, Bai D, Hu X, et al. Robust and antibacterial polymer/mechanically exfoliated graphene nanocomposite fibers for biomedical applications. ACS Appl Mater Interfaces, 2018, 10: 3002–3010
35 Tas M, Altin Y, Bedeloglu A. Graphene and graphene oxide-coated polyamide monofilament yarns for fiber-shaped flexible electrodes. J Textile Institute, 2019, 110: 67–73
36 Chen J, Li Y, Huang L, et al. High-yield preparation of graphene oxide from small graphite flakes via an improved Hummers method with a simple purification process. Carbon, 2015, 81: 826–834
37 Zhai H, Xu L, Liu Z, et al. Twisted graphene fibre based breathable, wettable and washable anti-jamming strain sensor for underwater motion sensing. Chem Eng J, 2022, 439: 135502
38 Zhang X, Yang Z, Yang X, et al. Sustainable antibacterial surgical suture based on recycled silk resource by an internal combination of

inorganic nanomaterials. ACS Appl Mater Interfaces, 2023, 15: 29971–29981
39 Connell L S, Gabrielli L, Mahony O, et al. Functionalizing natural polymers with alkoxysilane coupling agents: Reacting 3-glycidoxypropyl trimethoxysilane with poly(γ-glutamic acid) and gelatin. Polym Chem, 2017, 8: 1095–1103
40 Neves A I S, Rodrigues D P, De Sanctis A, et al. Towards conductive textiles: Coating polymeric fibres with graphene. Sci Rep, 2017, 7: 4250
41 Park S K, Seong C Y, Piao Y. A simple dip-coating approach for preparation of three-dimensional multilayered graphene-metal oxides hybrid nanostructures as high performance lithium-ion battery electrodes. Electrochim Acta, 2015, 176: 1182–1190
42 Tan L, Li X, Wang Z, et al. Lightweight reduced graphene oxide@-MoS_2 interlayer as polysulfide barrier for high-performance lithium–sulfur batteries. ACS Appl Mater Interfaces, 2018, 10: 3707–3713
43 Cui M, Ren S, Zhao H, et al. Polydopamine coated graphene oxide for anticorrosive reinforcement of water-borne epoxy coating. Chem Eng J, 2018, 335: 255–266
44 Liang B, Liu K, Liu P, et al. Organic salt-assisted liquid-phase shear exfoliation of expanded graphite into graphene nanosheets. J Materiomics, 2021, 7: 1181–1189
45 Palaskar S, Kale K H, Nadiger G S, et al. Dielectric barrier discharge plasma induced surface modification of polyester/cotton blended fabrics to impart water repellency using HMDSO. J Appl Polym Sci, 2011, 122: 1092–1100
46 Regis J, Vargas S, Irigoyen A, et al. Near-UV light assisted green reduction of graphene oxide films through *L*-ascorbic acid. Int J Smart Nano Mater, 2021, 12: 20–35
47 Liu K, Zhang J J, Cheng F F, et al. Green and facile synthesis of highly biocompatible graphene nanosheets and its application for cellular imaging and drug delivery. J Mater Chem, 2011, 21: 12034–12040
48 Liu J, Zhang J, Zhao Z, et al. A negative-response strain sensor towards wearable microclimate changes for body area sensing networks. Chem Eng J, 2023, 459: 141628
49 Zulan L, Zhi L, Lan C, et al. Reduced graphene oxide coated silk fabrics with conductive property for wearable electronic textiles application. Adv Elect Mater, 2019, 5: 1800648
50 Xu L, Liu Z, Zhai H, et al. Moisture-resilient graphene-dyed wool fabric for strain sensing. ACS Appl Mater Interfaces, 2020, 12: 13265–13274
51 Li Y, Lin D, Li Y, et al. Nonradical-dominated peroxymonosulfate activation through bimetallic Fe/Mn-loaded hydroxyl-rich biochar for efficient degradation of tetracycline. Nano Res, 2023, 16: 155–165
52 Fang M, Xiong X, Hao Y, et al. Preparation of highly conductive graphene-coated glass fibers by sol-gel and dip-coating method. J Mater Sci Tech, 2019, 35: 1989–1995
53 Giasuddin A B M, Britt D W. Microwave assisted sol-gel synthesis of silica-spider silk composites. Molecules, 2019, 24: 2521
54 Bhattacharjee S, Macintyre C R, Bahl P, et al. Reduced graphene oxide and nanoparticles incorporated durable electroconductive silk fabrics. Adv Mater Inter, 2020, 7: 2000814
55 Tian Y, Wu Q, Li F, et al. A flexible and biocompatible bombyx mori silk fibroin/wool keratin composite scaffold with interconnective porous structure. Colloids Surfs B-Biointerfaces, 2021, 208: 112080
56 Cai G, Xu Z, Yang M, et al. Functionalization of cotton fabrics through thermal reduction of graphene oxide. Appl Surf Sci, 2017, 393: 441–448
57 Wu Q, He C, Wang X, et al. Sustainable antibacterial surgical suture using a facile scalable silk-fibroin-based berberine loading system. ACS BioMater Sci Eng, 2021, 7: 2845–2857
58 Wan S, Li Y, Mu J, et al. Sequentially bridged graphene sheets with high strength, toughness, and electrical conductivity. Proc Natl Acad Sci USA, 2018, 115: 5359–5364
59 Ma L, Wu R, Patil A, et al. Acid and alkali-resistant textile triboelectric nanogenerator as a smart protective suit for liquid energy harvesting and self-powered monitoring in high-risk environments. Adv Funct Mater, 2021, 31: 2102963
60 Hu X, Xia X X, Huang S C, et al. Development of adhesive and conductive resilin-based hydrogels for wearable sensors. Biomacromolecules, 2019, 20: 3283–3293
61 Wang C, Xia K, Wang H, et al. Advanced carbon for flexible and wearable electronics. Adv Mater, 2019, 31: 1801072
62 Huang W, Ling S, Li C, et al. Silkworm silk-based materials and devices generated using bio-nanotechnology. Chem Soc Rev, 2018, 47: 6486–6504
63 Zhang J, Liu J, Zhao Z, et al. A facile scalable conductive graphene-coated Calotropis gigantea yarn. Cellulose, 2022, 29: 3545–3556
64 Li Y, Samad Y A, Taha T, et al. Highly flexible strain sensor from tissue paper for wearable electronics. ACS Sustain Chem Eng, 2016, 4: 4288–4295
65 Lu Y, Biswas M C, Guo Z, et al. Recent developments in bio-monitoring via advanced polymer nanocomposite-based wearable strain sensors. Biosens Bioelectron, 2019, 123: 167–177
66 Srimaneepong V, Skallevold H E, Khurshid Z, et al. Graphene for antimicrobial and coating application. Int J Mol Sci, 2022, 23: 499
67 Meng Q, Liu Z, Cai R, et al. Non-oxidized graphene/elastomer composite films for wearable strain and pressure sensors with ultra-high flexibility and sensitivity. Polyms Adv Techs, 2020, 31: 214–225
68 Zhang G J, Guo X X, Wang S L, et al. New graphene fiber coating for volatile organic compounds analysis. J Chromatography B, 2014, 969: 128–131
69 Eda G, Mattevi C, Yamaguchi H, et al. Insulator to semimetal transition in graphene oxide. J Phys Chem C, 2009, 113: 15768–15771
70 Kaiser A B, Gómez-Navarro C, Sundaram R S, et al. Electrical conduction mechanism in chemically derived graphene monolayers. Nano Lett, 2009, 9: 1787–1792
71 Mattevi C, Eda G, Agnoli S, et al. Evolution of electrical, chemical, and structural properties of transparent and conducting chemically derived graphene thin films. Adv Funct Mater, 2009, 19: 2577–2583
72 Jung I, Dikin D A, Piner R D, et al. Tunable electrical conductivity of individual graphene oxide sheets reduced at "low" temperatures. Nano Lett, 2008, 8: 4283–4287
73 Moon I K, Lee J, Ruoff R S, et al. Reduced graphene oxide by chemical graphitization. Nat Commun, 2010, 1: 73
74 Cao C, Lin Z, Liu X, et al. Strong reduced graphene oxide coated *Bombyx mori* silk. Adv Funct Mater, 2021, 31: 2102923
75 Feng Y, Chen Y, Chen Y, et al. Intestinal stents: Structure, functionalization and advanced engineering innovation. BioMater Adv, 2022, 137: 212810
76 Chen H Y, Chen Z Y, Mao M, et al. Self-adhesive polydimethylsiloxane foam materials decorated with MXene/cellulose nanofiber interconnected network for versatile functionalities. Adv Funct Mater, 2023, 33: 2304927
77 Li S N, He X F, Zeng Z F, et al. Mechanically ductile, ionically conductive and low-temperature tolerant hydrogel enabled by high-concentration saline towards flexible strain sensor. Nano Energy, 2022, 103: 107789
78 Li S N, Yu Z R, Guo B F, et al. Environmentally stable, mechanically flexible, self-adhesive, and electrically conductive $Ti_3C_2T_X$ MXene hydrogels for wide-temperature strain sensing. Nano Energy, 2021, 90: 106502
79 Ni Q Y, He X F, Zhou J L, et al. Mechanical tough and stretchable quaternized cellulose nanofibrils/MXene conductive hydrogel for flexible strain sensor with multi-scale monitoring. J Mater Sci Tech, 2024, 191: 181–191
80 Yang Z, Pang Y, Han X, et al. Graphene textile strain sensor with negative resistance variation for human motion detection. ACS Nano, 2018, 12: 9134–9141